Ultra-sparse dielectric nanowire grids as wideband reflectors and polarizers

Jae Woong Yoon,[1,2] Kyu Jin Lee,[1] and Robert Magnusson[1,*]

[1]*Department of Electrical Engineering, University of Texas at Arlington, Arlington, TX 76019, USA*
[2]*Department of Physics, Hanyang University, Seoul 133-791, South Korea*
[*]*magnusson@uta.edu*

Abstract: Engaging both theory and experiment, we investigate resonant photonic lattices in which the duty cycle tends to zero. Corresponding dielectric nanowire grids are mostly empty space if operated as membranes in vacuum or air. These grids are shown to be effective wideband reflectors with impressive polarizing properties. We provide computed results predicting nearly complete reflection and attendant polarization extinction in multiple spectral regions. Experimental results with Si nanowire arrays with 10% duty cycle show ~200-nm-wide band of high reflection for one polarization state and free transmission for the orthogonal state. These results agree quantitatively with theoretical predictions. It is fundamentally extremely significant that the wideband spectral expressions presented can be generated in these minimal systems.

OCIS codes: (310.6628) Subwavelength structures, nanostructures; (130.5440) Polarization-selective devices; (260.5740) Resonance; (130.2790) Guided waves.

References and links

1. P. Vincent and M. Neviere, "Corrugated dielectric waveguides: a numerical study of the second-order stop bands," Appl. Phys. (Berl.) **20**(4), 345–351 (1979).
2. L. Mashev and E. Popov, "Zero order anomaly of dielectric coated gratings," Opt. Commun. **55**(6), 377–380 (1985).
3. I. A. Avrutsky and V. A. Sychugov, "Reflection of a beam of finite size from a corrugated waveguide," J. Mod. Opt. **36**(11), 1527–1539 (1989).
4. R. Magnusson and S. S. Wang, "New principle for optical filters," Appl. Phys. Lett. **61**(9), 1022–1024 (1992).
5. Y. Ding and R. Magnusson, "Resonant leaky-mode spectral-band engineering and device applications," Opt. Express **12**(23), 5661–5674 (2004).
6. M. Streshinsky, R. Shi, A. Novack, R. T. P. Cher, A. E.-J. Lim, P. G.-Q. Lo, T. Baehr-Jones, and M. Hochberg, "A compact bi-wavelength polarization splitting grating coupler fabricated in a 220 nm SOI platform," Opt. Express **21**(25), 31019–31028 (2013).
7. M. A. Ahmed, M. Haefner, M. Vogel, C. Pruss, A. Voss, W. Osten, and T. Graf, "High-power radially polarized Yb:YAG thin-disk laser with high efficiency," Opt. Express **19**(6), 5093–5104 (2011).
8. J. Zhao, B. Li, H. Zhao, W. Wang, Y. Hu, S. Liu, and Y. Wang, "Generation of azimuthally polarized beams in fast axial flow CO_2 laser with hybrid circular subwavelength grating mirror," Appl. Opt. **53**(17), 3706–3711 (2014).
9. D. P. Biss, K. S. Youngworth, and T. G. Brown, "Dark-field imaging with cylindrical-vector beams," Appl. Opt. **45**(3), 470–479 (2006).
10. U. Levy, C. H. Tsai, L. Pang, and Y. Fainman, "Engineering space-variant inhomogeneous media for polarization control," Opt. Lett. **29**(15), 1718–1720 (2004).
11. T. Kämpfe, P. Sixt, D. Renaud, A. Lagrange, F. Perrin, and O. Parriaux, "Segmented subwavelength silicon gratings manufactured by high productivity microelectronic technologies for linear to radial/azimuthal polarization conversion," Opt. Eng. **53**(10), 107105 (2014).
12. Y. Ohtera, T. Sato, T. Kawashima, T. Tamamura, and S. Kawakami, "Photonic crystal polarization splitters," Electron. Lett. **35**(15), 1271–1272 (1999).
13. R.-C. Tuan, A. A. Salvekar, H.-P. Chou, C.-C. Chen, A. Scherer, P.-C. Sun, F. Xu, and Y. Fainman, "Design, fabrication, and characterization of form-birefringent multilayer polarizing beam splitter," J. Opt. Soc. Am. A **14**(7), 1627–1636 (1997).
14. D. Delbeke, R. Baets, and P. Muys, "Polarization-selective beam splitter based on a highly efficient simple binary diffraction grating," Appl. Opt. **43**(33), 6157–6165 (2004).

#248883 Received 28 Aug 2015; revised 12 Oct 2015; accepted 23 Oct 2015; published 27 Oct 2015

15. K. J. Lee, J. Curzan, M. Shokooh-Saremi, and R. Magnusson, "Resonant wideband polarizer with single silicon layer," Appl. Phys. Lett. **98**(21), 211112 (2011).
16. K. J. Lee, J. Giese, L. Ajayi, R. Magnusson, and E. Johnson, "Resonant grating polarizers made with silicon nitride, titanium dioxide, and silicon: design, fabrication, and characterization," Opt. Express **22**(8), 9271–9281 (2014).
17. R. Magnusson and M. Shokooh-Saremi, "Physical basis for wideband resonant reflectors," Opt. Express **16**(5), 3456–3462 (2008).
18. V. Karagodsky, F. G. Sedgwick, and C. J. Chang-Hasnain, "Theoretical analysis of subwavelength high contrast grating reflectors," Opt. Express **18**(16), 16973–16988 (2010).
19. M. G. Moharam, E. B. Grann, D. A. Pommet, and T. K. Gaylord, "Formulation for stable and efficient implementation of the rigorous coupled-wave analysis of binary gratings," J. Opt. Soc. Am. A **12**(5), 1068–1076 (1995).
20. S. M. Rytov, "Electromagnetic properties of a finely stratified medium," Sov. Phys. JETP **2**, 466–475 (1956).
21. D. Rosenblatt, A. Sharon, and A. A. Friesem, "Resonant grating waveguide structures," IEEE J. Quantum Electron. **33**(11), 2038–2059 (1997).
22. C. J. Chang-Hasnain and W. Yang, "High-contrast gratings for integrated optoelectronics," Adv. Opt. Photonics **4**(3), 379–440 (2012).
23. R. Magnusson, "Wideband reflectors with zero-contrast gratings," Opt. Lett. **39**(15), 4337–4340 (2014).
24. E. D. Palik, *Handbook of Optical Constants of Solids* (Academic, 1985).
25. P. H. Bolivar, M. Brucherseifer, J. G. Rivas, R. Gonzalo, I. Ederra, A. L. Reynolds, M. Holker, and P. de Maagt, "Measurement of the dielectric constant and loss tangent of high dielectric-constant materials at terahertz frequencies," IEEE Trans. Microw. Theory Tech. **51**(4), 1062–1066 (2003).
26. C. C. Homes, T. Vogt, S. M. Shapiro, S. Wakimoto, and A. P. Ramirez, "Optical response of high-dielectric-constant perovskite-related oxide," Science **293**(5530), 673–676 (2001).
27. Y. He, S. He, J. Gao, and X. Yang, "Nanoscale metamaterial optical waveguides with ultrahigh refractive indices," J. Opt. Soc. Am. B **29**(9), 2559–2566 (2012).
28. M. Choi, S. H. Lee, Y. Kim, S. B. Kang, J. Shin, M. H. Kwak, K.-Y. Kang, Y.-H. Lee, N. Park, and B. Min, "A terahertz metamaterial with unnaturally high refractive index," Nature **470**(7334), 369–373 (2011).

1. Introduction

Many innovative device concepts in nanoplasmonics and nanophotonics rely on intricate resonance effects generated with thin nanopatterned films. As incident light couples to the film, attendant resonance effects impose diverse spectral signatures on the output light. The guided-mode resonance concept refers to quasi-guided, or leaky, waveguide modes induced in periodic layers [1–5]. Whereas the fundamental resonance effect arises in any diffraction regime, subwavelength architectures enable the most useful spectra. Even though these effects have been known for a long time, new attributes and application possibilities continue to appear. In this paper, engaging similar resonance effects, we study photonic lattices with minimal material embodiments. From fundamental scientific viewpoints, it is interesting to discover just how sparse a resonant nanogrid can become while still sustaining a resonance. From practical viewpoints, it is of interest to find out if there is any utility to be derived from such an exercise. Here, we are particularly interested in the reflection and polarizing properties of such ultra-sparse photonic lattices.

Polarizers are important for numerous applications in photonic systems. Whereas conventional polarizers based on natural birefringent crystals and thin-film multilayers are commonplace, nanostructured polarizers offer compact integrability, thermal stability and potentially improved performance in terms of extinction ratio and bandwidth. Taking advantage of these properties, nanostructured thin-film polarizers and polarizing beam splitters have been applied to integrated optical platforms [6], high-power laser machining [7,8], high-resolution confocal microscopy [9], space-variant vector-beam generation [10,11], and many others. In early works, such elements were implemented by combining multilayer films with linear subwavelength gratings to induce polarization selectivity at normal incidence [12,13]. More advanced polarizer designs with reduced material embodiment and simple architecture were subsequently demonstrated engaging guided-mode resonance effects [14–16]. These devices operate with a broadband resonant reflection in one polarization state and concomitant transmission in the orthogonal state. It is widely assumed that large

#248883 Received 28 Aug 2015; revised 12 Oct 2015; accepted 23 Oct 2015; published 27 Oct 2015

refractive-index contrast and high average refractive index are necessary to support broadband performance with attendant multi-mode resonance excitation [17,18].

In complete contrast, here we show that ultra-sparse dielectric nanowire grids render remarkable wideband total light reflection and efficient polarization selectivity. These attributes are enabled by a broadband resonance effect for a preferred polarization state and essential invisibility in the other polarization. In the context of conventional elements based on multilayer Bragg reflection [13] and multiple ridge mode interference [18], it is somewhat counterintuitive that a device with such minimal material manifestation can provide the striking effects observed. Hence, the proof-of-concept experimental demonstration provided is particularly relevant. It shows excellent quantitative agreement with theory. Our models therefore support pursuit of practical device design and implementation applying various available natural and engineered materials having high dielectric constants.

2. Theoretical analysis

A representative dielectric nanowire grid is illustrated in Fig. 1 along with its polarizing functionality. The structure is defined by the period Λ, wire fill factor (or duty cycle) F, height h, dielectric constant ε_1, and dielectric constant ε_0 of the host medium. Relative to the array geometry, transverse electric (TE) polarization corresponds to the electric field oscillating along the wire (y-axis) and the orthogonal polarization is denoted as transverse magnetic (TM) polarization. For ultra-sparse high-index nanowire grids where $F << 1$ and $\varepsilon_1 >> \varepsilon_0$, associated polarization selectivity arises in two fundamental aspects. First, there is a large difference in the diffraction strength between TE and TM polarizations. As a measure of the diffraction strength, we define the diffraction potential $V(q)$ for the q-th order diffraction process as the q-th Fourier-harmonic amplitude of the dielectric function $\varepsilon(x)$ for TE polarization and the reciprocal dielectric function $\varepsilon^{-1}(x)$ for TM polarization [19]. These diffraction potentials can be approximated for high-index contrast ($\varepsilon_1 >> \varepsilon_0$) as

$$V_{\mathrm{TE}}(q) = (\varepsilon_1 - \varepsilon_0) F \,\mathrm{sinc}(Fq) \approx \varepsilon_1 F \,\mathrm{sinc}(Fq), \tag{1}$$

$$V_{\mathrm{TM}}(q) = \left(\varepsilon_1^{-1} - \varepsilon_0^{-1}\right) F \,\mathrm{sinc}(Fq) \approx \varepsilon_0^{-1} F \,\mathrm{sinc}(Fq), \tag{2}$$

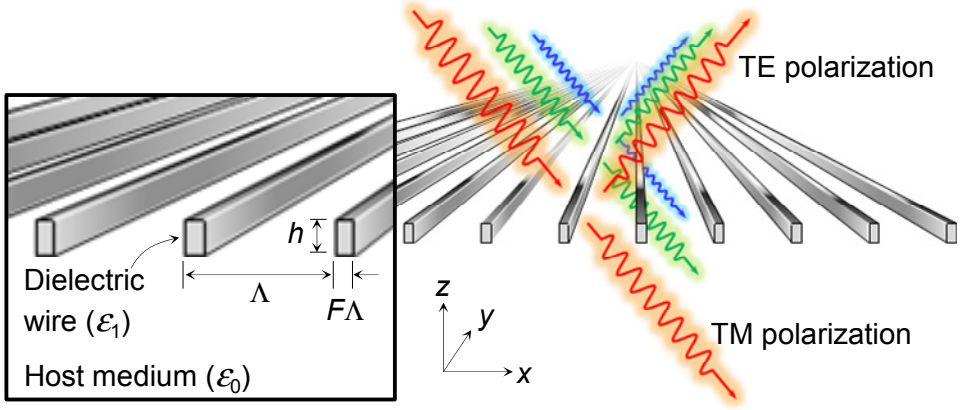

Fig. 1. Schematic illustration of an ultra-sparse TE reflector with concurrent TM invisibility.

where $\mathrm{sinc}(Fq) = \sin(\pi Fq)/(\pi Fq)$. The utility of the diffraction potential in the present context is that it relates directly to the fill factor F that is of central interest in the study of sparse photonic grids. Accordingly, we note that the TM diffraction potential $V_{\mathrm{TM}}(q)$ is vanishingly small for $F << 1$ regardless of ε_1 whereas the TE diffraction potential $V_{\mathrm{TE}}(q)$ can be persistently high if ε_1 is large enough to maintain a sizable $\varepsilon_1 F$ product. Second, the array's average refractive index in this limit also supports the generation of polarization contrast.

#248883 Received 28 Aug 2015; revised 12 Oct 2015; accepted 23 Oct 2015; published 27 Oct 2015

Using Rytov's effective medium theory [20], the zero-order effective refractive indices of the array for TE and TM polarizations are approximated as $n_{TE} \approx n_0(1 + \varepsilon_1 F/\varepsilon_0)^{1/2}$ and $n_{TM} \approx n_0(1 + F/2)$, respectively, where $n_0 = \varepsilon_0^{1/2}$. In these approximations, n_{TM} approaches the background refractive index n_0 for $F << 1$ regardless of the ε_1 value while n_{TE} is significantly larger than n_0 if the product $\varepsilon_1 F$ is comparable to or larger than ε_0.

In this picture, as $V_{TM}(q) << 1$ for all q, TM-polarized input light is not diffracted and consequently there exists no evanescent diffraction order in the nanogrid layer to generate a leaky mode. In addition, further exacerbating the situation, as the effective refractive index for TM-polarized light is close to that of the background, namely $n_{TM} \sim 1$ here, a guided mode cannot be supported. Therefore, neither of the conditions needed to generate a guided-mode resonance on the nanogrid is met and the TM-wave passes through the grid as a simple zero-order transmitted wave. In stark contrast, for TE-polarized input, there exists a nonvanishing diffraction potential $V_{TE}(q)$ capable of scattering the incident wave into evanescent diffraction orders $q = \pm 1, \pm 2, \ldots$ Simultaneously, there is sufficient material manifestation to support a guided mode owing to an appreciable value of the TE refractive index n_{TE}. Hence, TE-polarized light is both diffracted and guided and therefore capable of undergoing guided-mode resonance. This process further manifests as reradiated lateral Bloch modes creating a wideband zero-order reflectance in TE polarization on our subwavelength nanogrids as demonstrated in the remainder of this paper.

It is clear that the effects in play are enabled by the differences in the material manifestation of the device as experienced by the input light in alternate polarization states. This difference is conveniently and clearly expressible by the elementary diffraction potential and effective-medium theory as shown here. In the following analyses, we show how TE-polarized resonances and near-perfect TM invisibility in a dielectric nanowire grid produce a broad reflection band with efficient polarization selectivity when the cross-sectional wire fill factor F tends toward an extremely small value.

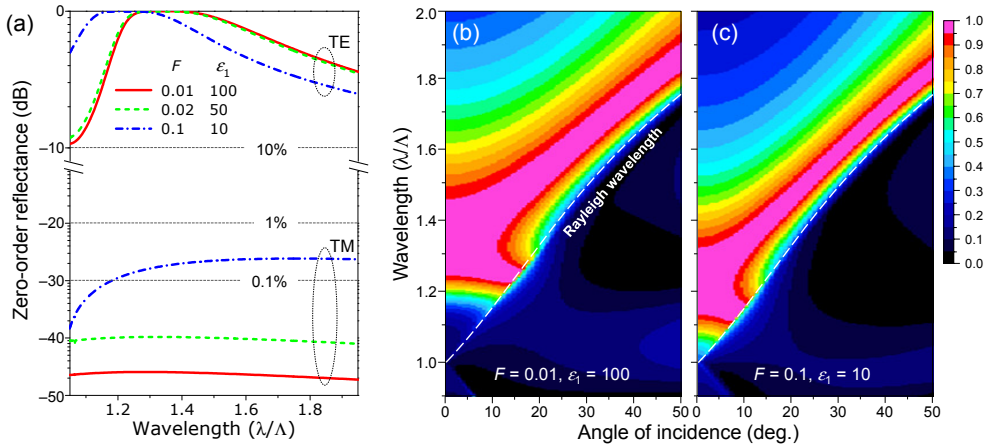

Fig. 2. Theoretical performance of ultra-sparse dielectric nanowire grid polarizers. (a) Zero-order TE and TM reflectance, R_0(TE) and R_0(TM), spectra under normal incidence for three different parameter sets (ε_1, F, h/Λ) = (100, 0.01, 0.315), (50, 0.02, 0.317), and (10, 0.1, 0.342). Angle-dependent R_0(TE) spectra for (b) (ε_1, F, h/Λ) = (100, 0.01, 0.315) and (c) (ε_1, F, h/Λ) = (10, 0.1, 0.342).

Using rigorous coupled-wave analysis (RCWA) [19], we numerically calculate the zero-order reflectance (R_0) spectra under TE- and TM-polarized light incidence for three example designs with parameter sets (ε_1, F, h/Λ) = (100, 0.01, 0.315), (50, 0.02, 0.317), and (10, 0.1, 0.342). We take free space ($\varepsilon_0 = 1$) as the host medium. In these examples, the product $\varepsilon_1 F$ is constant at 1 with wire height chosen to maximize the TE resonance reflectance. In Fig. 2(a),

#248883 Received 28 Aug 2015; revised 12 Oct 2015; accepted 23 Oct 2015; published 27 Oct 2015

the R_0(TE) spectra show broadband reflection over the normalized full-width at half-maximum bandwidth $\Delta\lambda/\Lambda$ ~20%. The normalized bandwidth of the reflection plateau where $R_0(\mathrm{TE}) \geq 0.99$ is $\Delta\lambda/\Lambda$ ~13% for all three cases. This broadband reflection occurs over a wide acceptance angle ~20° as shown in Figs. 2(b) and 2(c).

In contrast, as shown in Fig. 2(a), the TM reflectance R_0(TM) is well below 10^{-2} and essentially negligible. Note that R_0(TM) is less than 3×10^{-5} for $F = 0.01$ and $\varepsilon_1 = 100$. In more detail, R_0(TM) scales roughly with $2(n_{\mathrm{TM}}-n_0)^2/(n_{\mathrm{TM}} + n_0)^2 \approx F^2/4$ corresponding to the specular reflection from the homogeneous average effective film. Therefore, the polarization extinction ratio in reflection across the TE resonance bandwidth is approximately given by

$$R_0(\mathrm{TE}) / R_0(\mathrm{TM}) \approx 4F^{-2} \approx 4\varepsilon_1^2, \tag{3}$$

with the condition $\varepsilon_1 F \approx 1$ to maintain an appreciable TE diffraction potential. The TE and TM field distributions at the center wavelength of the TE-reflection plateau for the examples with parameter sets (ε_1, F, h/Λ) = (100, 0.01, 0.315) and (10, 0.1, 0.342) are shown in Figs. 3(a) and 3(b), respectively. In each case, there is a clear resonant field enhancement in the array for TE polarization whereas TM-polarized light propagates freely through the device without significant perturbation of the propagating wavefronts.

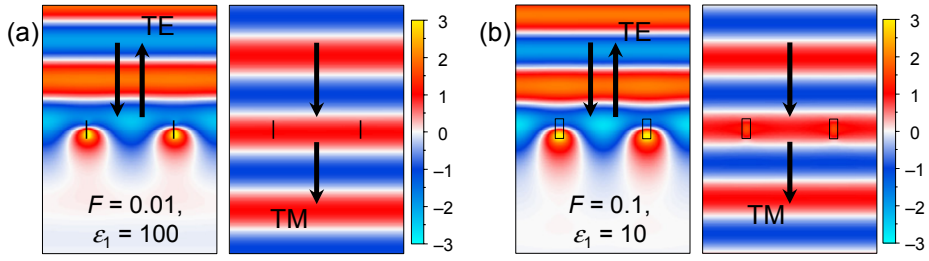

Fig. 3. (a) Field distributions under TE (left panel) and TM (right panel) polarized light incidence for the parameter set (ε_1, F, h/Λ) = (100, 0.01, 0.315) at wavelength $\lambda = 1.343\Lambda$. (b) Field distributions under TE (left panel) and TM (right panel) polarized light incidence for the parameter set (ε_1, F, h/Λ) = (10, 0.1, 0.342) at wavelength $\lambda = 1.224\Lambda$. The indicated fields are electric field for TE and magnetic field for TM. Their values are normalized by the incident field amplitude in both (a) and (b).

The devices presented herein operate under the guided-mode resonance effect. The broadband TE reflection is driven by resonant excitation and reradiation of lateral Bloch modes via one or more evanescent diffraction orders [21]. The generation of a wavevector directed along the + z-axis sustaining the propagation of the reflected wave is a diffractive effect and not related to reflections off grating ridge interfaces [18,22]. The nanogrids presented have exceedingly small fill factors and attendant thin grating ridges. They are capable of supporting only a single ridge mode. Thus, interference between multiple local ridge modes plays no causal roles in these devices [23].

3. Experimental verification

We experimentally demonstrate a Si-nanowire-grid polarizing beam splitter in the near-infrared region. The fabrication steps include sputtering a 540-nm-thick amorphous Si film on a 1-mm-thick microscope slide glass, ultraviolet laser interference lithography to form a photoresist grating mask, reactive-ion etching using a $CHF_3 + SF_6$ gas mixture, and post-etch O_2 ashing to remove residual photoresist. Figure 4(a) shows a photograph of nine fabricated devices on a 1×1 inch^2 substrate. Aiming for device operation in the telecommunications band over the 1300~1600 nm wavelength range, these devices have identical periods of Λ = 854.0 nm but slightly different fill factors such that F gradually decreases from 0.12 for the bottom-left device to 0.05 for the top-right device. Clearly visible is the semi-transparency in

#248883 Received 28 Aug 2015; revised 12 Oct 2015; accepted 23 Oct 2015; published 27 Oct 2015

the device areas due to the low Si-wire fill factor. The best performance is obtained with a device with $F = 0.1$. Figures 4(b)-4(d) show cross-sectional and top-view scanning electron microscope (SEM) images of this device. The measured geometrical parameters are indicated therein. To keep the original sample undestroyed, we took the cross-sectional micrographs in Fig. 4(b) from a sacrificial sample fabricated with an identical process while the top-view micrographs in Figs. 4(c) and 4(d) show the actual device whose optical spectrum is measured and presented here.

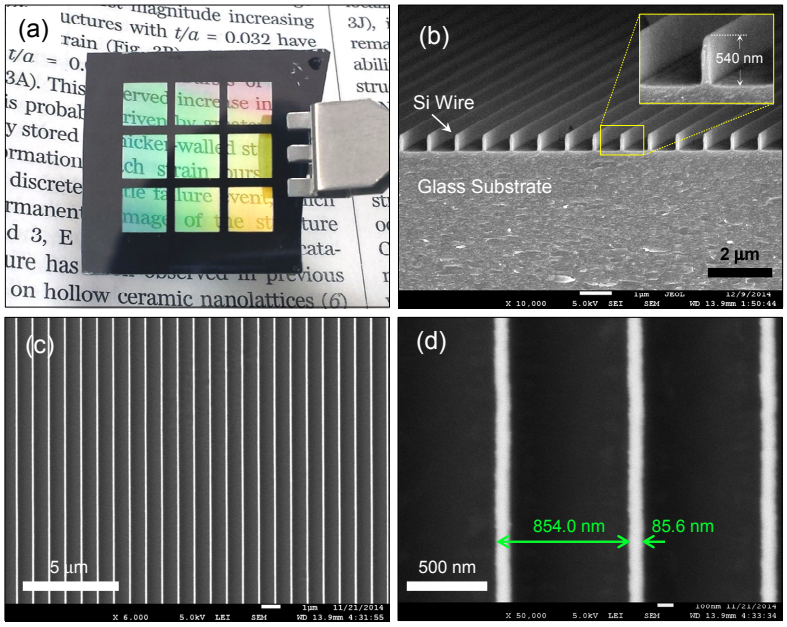

Fig. 4. Device fabrication and characterization. (a) A photograph of nine ultra-sparse Si nanowire grids with different Si-wire fill factors on a 1 × 1 inch^2 glass substrate. Cross-sectional (b) and top-view (c and d) SEM images of the device.

The fabricated sample is further prepared for spectral measurement. To establish an optically symmetric background environment, we place an index-matching fluid with refractive index 1.526 between the cover and substrate glass slides with refractive index 1.520. Thus the device is immersed in an approximately homogeneous host medium. Spectra are collected with an infrared spectrum analyzer (AQ6375, Yokogawa) and a supercontinuum light source (Koheras SuperK Compact, NKT Photonics). Figure 5 shows the measured TE and TM extinction ($1–T_0$) and reflectance (R_0) spectra in comparison with theoretical predictions. In the calculation, we apply the exact cross-sectional shape of the fabricated structure as shown in the insets of Figs. 5(c) and 5(d). We also use the experimental dielectric constant $\varepsilon_1 = 12.25$ of our Si film that we determine with ellipsometry (VASE Ellipsometer, J. A. Woollam). Shown in Figs. 5(a) and 5(b) are the TE and TM extinction spectra in experiment and theory, respectively. We note that the extinction for lossless systems must be identical to the reflectance, i.e., $1–T_0 = R_0$, in the zero-order regime above the Rayleigh wavelength (white dotted lines). There is excellent quantitative agreement between theory and experiment across the wide angular and wavelength ranges considered. Figures 5(c) and 5(d) show the measured and theoretical spectra for the TE extinction, TE reflectance, and TM reflectance at normal incidence. The TE reflection bandwidth for R_0(TE) > 0.9 is ~190 nm in the experiment and ~200 nm in the theory. We attribute the higher TM reflectance in the experiment to the specular reflections at the cover and substrate glass surfaces where about 4% of the incident optical power is reflected from each. In the theoretical spectrum in Fig.

#248883 Received 28 Aug 2015; revised 12 Oct 2015; accepted 23 Oct 2015; published 27 Oct 2015

5(d), the TM reflectance is below 0.5% over the wavelength region corresponding to the high TE-reflection plateau.

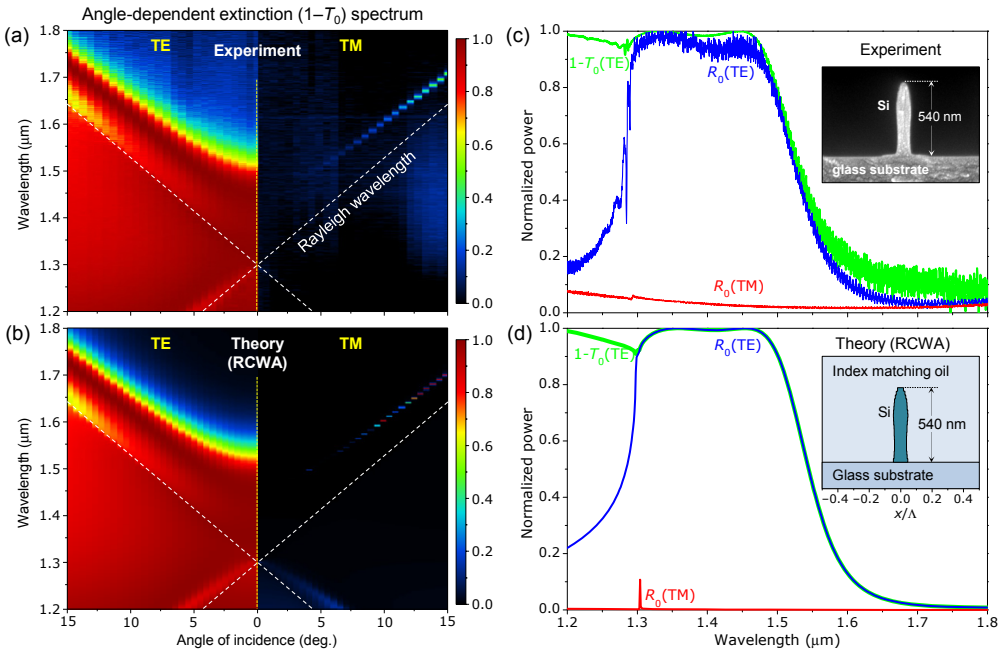

Fig. 5. Experimental performance of an ultra-sparse Si nanowire array reflector/polarizer. (a) Measured angle-dependent extinction (1–T_0) spectra under TE- and TM-polarized light incidence. (b) Calculated angle-dependent TE and TM extinction spectra for comparison. (c) Measured spectra of the TE reflectance R_0(TE), TM reflectance R_0(TM), and TE extinction (1–T_0). (d) Calculated spectra of the TE reflectance R_0(TE), TM reflectance R_0(TM), and TE extinction (1–T_0) for comparison.

4. Conclusions

In summary, applying both theory and experiment, we demonstrate the key properties of nanophotonic lattices built with extremely small fill factors. We show that attendant ultra-sparse dielectric nanowire grids strongly polarize incident light in reflection and transmission across considerable spectral and angular extents. As supported by elementary effective-medium arguments, the nanogrid array is essentially invisible to TM polarized light while resonating effectively in TE polarization. Importantly, this device idea is feasible in wide spectral domains including the near-infrared, THz, and longer wavelength regions. We note that various high-index materials are available to suit a given spectral region of interest. For example, semiconductors such as Si, GaAs, and Ge have dielectric constant in the range ε = 10~20 in the near-infrared and telecommunications bands [24]. For operation at longer wavelengths, much higher dielectric constants are available. $ZrSnTiO_3$ ceramics [25] and perovskite-related oxides [26] have ε ~100 in the THz domain. Artificial engineered materials are under development with hyperbolic metamaterials [27] for effective ε ~100 in the near-infrared domain and with H-shaped metallic patch arrays [28] for effective ε ~1000 at THz frequencies. Recalling Eq. (3), this value of dielectric constant implies a polarization extinction ratio ~4×10^6. Therefore, the proposed device class is promising to attain extreme polarization selectivity in various frequency domains.

#248883 Received 28 Aug 2015; revised 12 Oct 2015; accepted 23 Oct 2015; published 27 Oct 2015

Acknowledgments

R.M. conceived the original idea and designed the initial devices. K.J.L. fabricated the prototype devices. J.W.Y. performed sample characterization, spectral measurements, and computations. J.W.Y and R.M. wrote the paper.

The research leading to these results was supported in part by the Texas Instruments Distinguished University Chair in Nanoelectronics endowment. Additional support was provided by a UT System Texas Nanoelectronics Research Superiority Award funded by the State of Texas Emerging Technology Fund.

#248883 Received 28 Aug 2015; revised 12 Oct 2015; accepted 23 Oct 2015; published 27 Oct 2015